Dual-Chirp Photonics-Based Radar for Distance and Velocity Measurement Based on Compressive Sensing

Yujiao Ding, Shuxu Guo, Hao Wu, Di Wang, Jiaqi Li, *Member, IEEE*, Yang Yang, Fengtao Cui, and Wei Dong

***Abstract*—We proposed a dual-chirp microwave photonic radar based on compressive sensing for distance and velocity measurement. This radar can generate different chirp linear frequency modulated (LFM) signals using a dual-parallel Mach-Zehnder modulator (DPMZM). In the receiving part, a dual-drive Mach-Zehnder modulator (DDMZM) and a Mach-Zehnder modulator (MZM) are cascaded for the optical mixing and de-chirp processing with a pseudo-random bit sequence (PRBS). Then the mixed signal can be gathered by an analog-to-digital converter (ADC) at a sampling rate that is well below the Nyquist sampling rate. Using fewer sampling points, the reconstruction algorithm can recover the de-chirped signal accurately with a compression ratio of 8. A proof-of-concept experiment demonstrates that when the target is stationary, the distance measurement error is about 1.560 cm. The signal-to-noise ratio (SNR) of the recovery signal is enhanced to 30.725 dB. When the target is moving, the simulation results present that the maximum distance error is 1.2 cm, and the velocity error is below 0.140 m/s. This compressive sensing radar reduces the pressure of a massive amount of data storage or processing and guarantees the accuracy of signal recovery. At the same time, it breaks the limitation of operation bandwidth and increases the speed of operation.**

***Index Terms*—Compressive sensing, microwave radar, sub-Nyquist sampling, optical mixing.**

I. Introduction

RADAR is used for collecting location information and real-time imaging of an object in many scenes [1], [2]. Recently, microwave photonic techniques have been brought to radar systems because of the advantages such as broad bandwidth, fast analog signal processing, and electromagnetic interference (EMI) immunity [3], [4]. The linear frequency modulation (LFM) signals have been widely used in radar systems [5], [6]. However, for a single-chirp signal, the ambiguity function is knife-edge typed, with large range-Doppler coupling, which can decrease the range-Doppler resolution. Therefore, the dual-chirp signal is desired to be generated because it causes less range-Doppler coupling and can be generated based on photonics approaches, such as using a dual-polarization quadrature phase-shift keying (DP-QPSK) modulator [7], a dual-drive Mach-Zehnder modulator (DDMZM) [8], [9], or two cascaded Mach-Zehnder modulators (MZMs) [10].

In the receiving part of a radar, the de-chirping process of the echo signal can be realized by DDMZM [11] or phase modulator (PM) [12]. The de-chirped signal, which carries the distance's information, can be collected by analog-to-digital converters (ADCs). The frequency of the de-chirped signal is proportional to the transmitted LFM signal's rate and the distance of the target. However, with the use of wide bandwidth transmitted signals and the remote target measurement, the Nyquist sampling rate can be high and is well beyond the scope of the ADC. At the same time, the large amount of data that radar systems usually dispose of would significantly expand the ADCs' data storage capacity. In the radar system, the target shows a high degree of sparsity compared with the background. Compressive sensing (CS) is a practical approach to sampling sparse signals with a low sampling rate and few sampling points, reducing unnecessary data storage. It contains signal mixing, compressive sampling, and reconstruction process. To realize CS, microwave photonic techniques have large bandwidth and flexible structures. For example, two cascaded MZMs and a balanced photodetector (BPD) are used to recognize radio frequency (RF) signals precisely [13]. In [14], the IQ modulator is used to recover rectangular pulse with a 520-MHz ADC. The photonic RF channelization system decreases the speed of random sequences with parallel MZMs and photodetectors (PDs) [15]. The reconstruction algorithm has developed in recent years. Orthogonal matching pursuit (OMP) is widely used for signal recovery [16]. Based on the OMP algorithm, many optimized schemes appear, such as r-OMP [17] and regularized OMP (ROMP) algorithm [18], and compressive sampling matching pursuit (CoSaMP) algorithm [19], [20]. Compared with the OMP algorithm used before, the ROMP, r-OMP, and CoSaMP algorithms develop the calculation speed. In addition, the CoSaMP algorithm would throw

Manuscript received 27 June 2022; accepted 3 July 2022. Date of publication 6 July 2022; date of current version 27 July 2022. This work was supported by the National Natural Science Foundation of China under Grant 61875070. *(Corresponding author: Wei Dong.)*

Yujiao Ding, Shuxu Guo, Hao Wu, Di Wang, and Wei Dong are with the State Key Laboratory on Integrated Optoelectronics, College of Electronic Science & Engineering, Jilin University, Changchun 130012, China (e-mail: dingyj20@mails.jlu.edu.cn; guosx@jlu.edu.cn; haowu21@mails.jlu.edu.cn; 1913584528@qq.com; dongw@jlu.edu.cn).

Jiaqi Li is with Shanghai Radio Equipment Research Institute, Shanghai 201109, China (e-mail: jlu_ljq@163.com).

Yang Yang and Fengtao Cui are with Changchun Automotive Test Center Company, Ltd, Changchun 130012, China (e-mail: yangyang@catc.com.cn; cuifengtao@catc.com.cn).

Digital Object Identifier 10.1109/JPHOT.2022.3188846

This work is licensed under a Creative Commons Attribution-NonCommercial-NoDerivatives 4.0 License. For more information, see https://creativecommons.org/licenses/by-nc-nd/4.0/

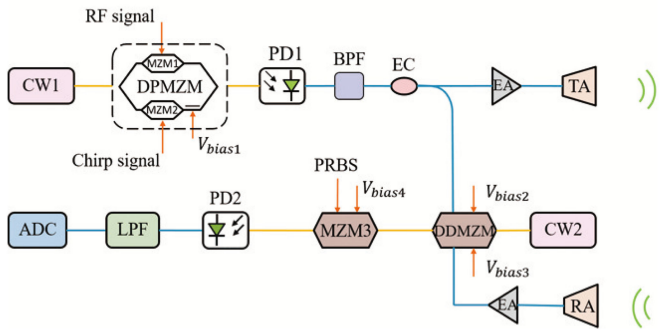

Fig. 1. The schematic of the proposed radar system. CW: continuous wave; RF: radiofrequency; MZM: Mach-Zehnder modulator; DPMZM: dual-parallel Mach-Zehnder modulator; PD: photodetector; BPF: band-pass filter; EC: electrical coupler; TA: transmitting antenna; RA: receiving antenna; EA: electrical amplifier; DDMZM: dual-drive Mach-Zehnder modulator; LPF: low-pass filter; ADC: analog-to-digital converter; PRBS: pseudo-random bit sequence.

away redundant elements to develop the convergence speed. In the iterative process, it can reduce the storage place of the element library. So, this algorithm offers rigorous bounds on computational cost and improves reconstruction efficiency.

In this paper, a dual-chirp microwave photonic radar based on CS technology is proposed for the distance and velocity measurement. In the transmitted part, a dual-parallel Mach-Zehnder modulator (DPMZM) is used to generate a dual-chirp signal. In the receiving part, a DDMZM is cascaded with an MZM to realize the de-chirping process and signal mixing. The mixed-signal after the low-pass filter (LPF) is compressively sampled and digitized at a sub-Nyquist rate. Finally, the CoSaMP algorithm can reconstruct the de-chirped signal accurately, and the distance or velocity information can be obtained by the frequency spectrum of the recovered signal. Compared with our previous work [21], the generation of a dual-chirp microwave waveform has a much smaller Doppler coupling which gives a high range-Doppler resolution. Moreover, the central frequency and the bandwidth of the transmitted signal can be altered flexibly by adjusting the two signals injected into the DPMZM. Then, in the receiver, the use of DDMZM and MZM realizes the de-chirping and the signal mixing process, avoiding high-speed electronics. The compressed signal collected by the low-speed ADC releases the pressure of downlink data storage and improves the performance of the recovered frequency spectrum. In our experiment and simulation, when the compression ratio is 8, the recovery algorithm can reconstruct the de-chirped signal accurately. In the experiment for a static target, the maximum distance error is about 1.560 cm, and the signal-to-noise ratio (SNR) can be developed to 30.725 dB. When the velocity is added to the echo signal in the simualtion, the maximum distance error is 1.2 cm, and the velocity error is less than 0.140 m/s.

II. Principles

Fig. 1 demonstrates the block diagram of the dual-chirp radar system. In the transmitter of the system, a continuous wave (CW) light wave at $\omega_0 = 2\pi f_0$ from the laser (CW1) is injected into a DPMZM. The amplitude of the optical carrier is set as E_{in}. There are two sub-MZMs in the DPMZM (MZM1 and MZM2). An RF signal at ω_1 is generated by a signal source and injected into the MZM1. A chirp signal $\cos(\omega_2 t + kt^2/2)$ is applied to the MZM2, in which ω_2 and k are the center angular frequency and the chirp rate, respectively. MZM1 and MZM2 are biased at the minimum transmission point (MITP) to achieve a double-sideband suppressed-carrier modulation. So, the optical output field of DPMZM can be given as follows [21]:

$$E_1(t) = E_{in}\begin{bmatrix} J_1(\beta_1)\, e^{j(\omega_0-\omega_1)t} \\ +J_1(\beta_1)\, e^{j(\omega_0+\omega_1)t} \\ +J_1(\beta_2)\, e^{j\left(\omega_0 t-\omega_2 t-\frac{kt^2}{2}+\varphi_1\right)} \\ +J_1(\beta_2)\, e^{j\left(\omega_0 t+\omega_2 t+\frac{kt^2}{2}+\varphi_1\right)} \end{bmatrix}, \quad (1)$$

where J_n is the n^{th}-order of the first kind Bessel function. β_1 and β_2 are the modulation index of MZM1 and MZM2. φ_1 is the fixed phase caused by the lower arm with a voltage of $V_{\text{bias 1}}$. After PD1, the electric field can be expressed as:

$$\begin{aligned} i_1(t) \propto\ & 2J_1^2(\beta_1)\cos\left(2\omega_2 t + kt^2\right) + 2J_1^2(\beta_2)\cos(2\omega_1 t) \\ & + 4J_1(\beta_1)J_1(\beta_2)\cos(\varphi_1)\cos\left(\omega_1 t - \omega_2 t - \frac{kt^2}{2}\right) \\ & + 4J_1(\beta_1)J_1(\beta_2)\cos(\varphi_1)\cos\left(\omega_1 t + \omega_2 t + \frac{kt^2}{2}\right), \end{aligned} \quad (2)$$

when $V_{\text{bias 1}}$ is set properly, $\varphi_1 = 0$, and the frequency components of $2\omega_1$ and $(2\omega_2 t + kt^2)$ can be filtered after the band-pass filter (BPF). So, $i(t)$ can be simplified as:

$$i_1(t) \propto 4J_1(\beta_1)J_1(\beta_2)\begin{bmatrix} \cos\left(\omega_1 t - \omega_2 t - \frac{kt^2}{2}\right) \\ +\cos\left(\omega_1 t + \omega_2 t + \frac{kt^2}{2}\right) \end{bmatrix}, \quad (3)$$

A dual-chirp LFM signal can be achieved. The carrier frequency is ω_1 and can be adjusted freely. The bandwidth is related to the single-chirp signal. The instantaneous frequency of $i(t)$ can be formulated as:

$$f_T(t) = \begin{cases} f_1 - kt \\ f_2 + kt \end{cases} t \in [(n-1)T, nT], \quad (4)$$

where f_1 and f_2 are the initial frequencies of the two bands of the generated signal; T is the duration time. An electrical coupler (EC) is used to divide the electric signal into two branches. One is sent to the transmitting antenna after the electrical amplifier (EA); the other is applied to the DDMZM. The echo signal can be collected by the receiving antenna and then injected into the DDMZM. The angular frequency of the light wave generated from CW2 is ω_0. The frequency of the echo signal is written as:

$$f_E(t) = \begin{cases} f_1 - k(t-\Delta\tau) \\ f_2 + k(t-\Delta\tau) \end{cases} t \in [(n-1)T, nT], \quad (5)$$

where $\Delta\tau$ is the delay time between the transmitting and the receiving antenna. The optical output field of the DDMZM can

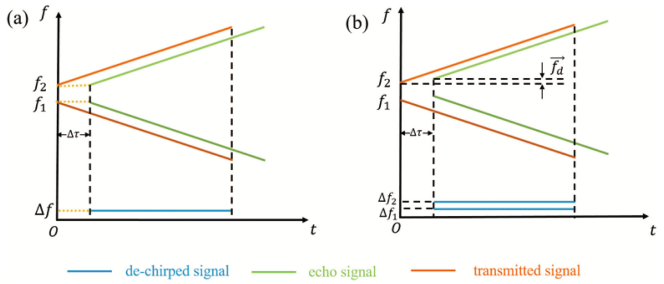

Fig. 2. Frequency-time diagram of the transmitted and echo signal. (a) static target. (b) moving target.

be represented as [11]:

$$E_{DDMZM}(t) = E_{in} J_0^2(m_2) \cos\left(\frac{\varphi_2}{2}\right) e^{j(\omega_0 t + \varphi_2/2)} + \frac{E_{in}}{2} J_0(m_2) J_1(m_2) \left\{ \begin{array}{c} e^{j\left(\omega_o t + 2\pi f_T(t) t + \frac{\pi}{2}\right)} \\ -e^{j\left(\omega_o t - 2\pi f_T(t) t - \frac{\pi}{2}\right)} \\ +e^{j\left(\omega_o t + 2\pi f_E(t) t + \frac{\pi}{2} + \varphi_2\right)} \\ -e^{j\left(\omega_o t - 2\pi f_E(t) t - \frac{\pi}{2} + \varphi_2\right)} \end{array} \right\} \quad (6)$$

The DDMZM is biased at the MITP. m_2 and φ_2 represent the modulation index and the phase difference between the two arms, respectively. Under the small-signal modulation, only the first-order sidebands are considered and $\varphi_2 = k\pi, (k = 0, \pm 1, \pm 2, \ldots)$. The optical power after DDMZM is:

$$P_{\text{out}\,1} \propto P_{\text{in}} \left[\cos\left(2\pi \left| f_T(t) - f_E(t) \right| t\right)\right]. \quad (7)$$

The component of $\cos(2\pi|f_T(t) - f_E(t)|t)$ is defined as the de-chirped signal, and the frequency component of $|f_T(t) - f_E(t)|$ is defined as Δf. As Fig. 2(a) shows, $\Delta f = k\Delta\tau$. At this moment, the distance of the target can be calculated as:

$$R = \frac{c \cdot \Delta\tau}{2} = \frac{c \cdot \Delta f}{2\,k}, \quad (8)$$

where c is the velocity of the light in the vacuum. If the target is moving, the echo signal will have a frequency offset compared to the transmitted signal. The frequency shift is the Doppler frequency shift (DFS) $\overrightarrow{f_d}$ and $f'_E(t) = f_E(t) + \overrightarrow{f_d}$. In Fig. 2(b), for a moving target, the frequency component of $|f_T(t) - f_E(t)|$ can be expressed as:

$$\Delta f_1 = k\Delta\tau - \overrightarrow{f_d}, \quad (9)$$

$$\Delta f_2 = k\Delta\tau + \overrightarrow{f_d}. \quad (10)$$

So, the distance and the velocity of the target can be derived as:

$$R = \frac{c \cdot \Delta\tau}{2} = \frac{c \cdot (\Delta f_1 + \Delta f_2)}{4k}, \quad (11)$$

$$|v| = \frac{\lambda \cdot \left|\overrightarrow{f_d}\right|}{2} = \frac{\lambda \left|\Delta f_2 - \Delta f_1\right|}{4}. \quad (12)$$

Then the optical signal output from DDMZM is emitted to the MZM3 for the optical mixing process. The PRBS from another source is injected into MZM3. If the time domain signal of PRBS is defined as $r(t)$, respectively, the output optical power of MZM3 is

$$P_{\text{out}\,2} = \frac{P_{\text{out}\,1}}{2} \cdot \left[1 + \cos\left(\pi \frac{V_{r(t)} + V_{\text{bias}\,4}}{V_\pi}\right)\right], \quad (13)$$

where $V_{r(t)}$ is the amplitude of the PRBS, $V_{\text{bias}4}$ and V_π is the bias voltage and the half-wave voltage applied to MZM3, respectively. By adjusting MZM3 bias at the quadrature point and under a small signal modulation, $P_{\text{out}\,2}$ is simplified as:

$$P_{\text{out}\,2} \approx \frac{P_{\text{out}\,1}}{2}\left[1 + \pi \frac{V_{r(t)}}{V_\pi}\right]. \quad (14)$$

Then the optical signal is detected by PD2 and the electrical signal is written as:

$$I(t) \propto \left[\cos\left(2\pi \left| f_T(t) - f_E(t) \right| t\right)\right]\left[1 + \gamma r(t)\right], \quad (15)$$

γ refers to the modulation index of MZM3. So, $I(t)$ consists of two parts: the de-chirped signal $\cos(2\pi|f_T(t) - f_E(t)|t)$ which is defined as $x(t)$, and $\gamma r(t)\cos(2\pi|f_T(t) - f_E(t)|t)$, which is the multiplication term between $x(t)$ and $r(t)$. The LPF is used to filter the part of $x(t)$. The multiplication term, which carries the information of the de-chirped signal, is left to downsampled and digitized by the ADC.

The CS can be expressed as reconstructing the unknown signal u from the less observed signal y. u contains N points and $u = W\theta$, where W is an $N \times N$ orthonormal basis matrix, θ is an $N \times 1$ vector which is the sparse demonstration of u. The process of CS can be expressed as:

$$y = \Phi u = DHRW\theta, \quad (16)$$

where y is the observed signal which contains M points ($M \ll N$). D is the $M \times N$ matrix which is related to the compression ratio. If the compression ratio is defined as δ, $\delta = N/M$. H is an $N \times N$ matrix that corresponds to the LPF. R is the $N \times N$ diagonal matrix representing the PRBS. According to solve the minimum ℓ_1 norm reconstruction:

$$\hat{\theta} = \text{argmin}\,\|\theta\|_{\ell_1}, \quad \text{subject to } \Phi W\theta = y. \quad (17)$$

We can acquire an optimal estimation of θ. Next, the estimation result u can be calculated. For signal reconstruction, the CoSaMP algorithm is applied to realize the reconstruction process. It requires only matrix-vector multiplies with the sampling matrix so it decreases the complexity of calculation and increases the calculating speed. In a radar system, the observed signal can be regarded as y and acquired by the low-speed ADC; the de-chirp signal $x(t)$ can be regarded as u and can be recovered through the recovery algorithm.

III. Results and Discussions

To evaluate the performance of the proposed radar scheme, an experiment based on Fig. 1 is established. The wavelength of CW1 (Santac TLS-510) is 1550 nm and sent to the DPMZM, with a power of 20 mW. The RF signal from a signal generator (Keysight E8257D) at 9 GHz is applied to MZM1; an arbitrary waveform generator (AWG) (Keysight M8196 A) provides the chirp signal and sends it to MZM2. MZM1 and MZM2 are working at MITP. The frequency range and the amplitude of the LFM signal are from 0.2 GHz to 1.2 GHz and 1 V, respectively.

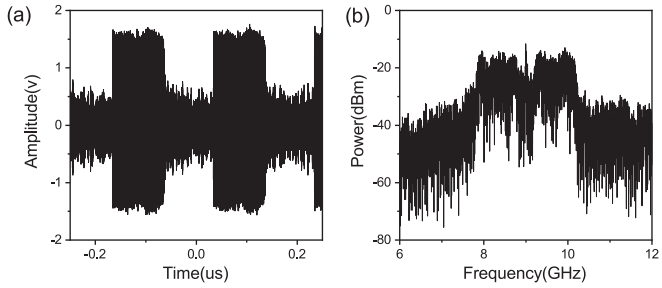

Fig. 3. Dual-chirp LFM signal. (a) temporal waveform; (b) frequency spectrum.

The time duration is 100 ns. The $V_{\text{bias 1}}$ is set properly, and the DPMZM is working to realize the double-sideband suppressed-carrier modulation. The responsivity of PD1 (KG-PD-50G-A-FC) is 0.55 A/W, and the 3-dB bandwidth is 50 GHz. After the PD1 and the BPF, the low-frequency term $\cos(2\omega_2 t + kt^2))$ and the high-frequency term $\cos(2\omega_1 t)$ are removed, after that the dual-chirp LFM signal is generated. The time-domain of the dual-chirp signal collected by the oscilloscope (Keysight MSOV254 A) and the frequency spectrum are shown in Fig. 3(a) and (b). The maximum sampling rate of the oscilloscope is 80 GSa/s. As Fig. 3(b) shown, the two bands of the LFM signal are 7.8 GHz-8.8 GHz and 9.2 GHz-10.2 GHz, respectively. Moreover, the bandwidth and central frequency of the dual-chirp signal can be adjusted freely according to ω_1, ω_2 and B.

The dual-chirp signal is used widely to decrease the range-Doppler coupling. For a single-chirp LFM signal, the ambiguity function is formulated as:

$$|\chi_s(\tau;\Omega_d)|^2 = \left|\left(1-\frac{|\tau|}{T}\right)\frac{\sin\left(\frac{1}{2}T\left(2\pi k\tau \pm \Omega_d\right)\left(1-\frac{|\tau|}{T}\right)\right)}{\frac{1}{2}T\left(2\pi k\tau \pm \Omega_d\right)\left(1-\frac{|\tau|}{T}\right)}\right|^2 \tag{18}$$

where $|\tau| \le T$. For a dual-chirp LFM signal, the ambiguity function is written as:

$$|\chi_d(\tau;\Omega_d)|^2 = \left|\begin{array}{c}\left(1-\frac{|\tau|}{T}\right)\frac{\sin\left(\frac{1}{2}T(2\pi k\tau+\Omega_d)\left(1-\frac{|\tau|}{T}\right)\right)}{\frac{1}{2}T(2\pi k\tau+\Omega_d)\left(1-\frac{|\tau|}{T}\right)} \\ +\left(1-\frac{|\tau|}{T}\right)\frac{\sin\left(\frac{1}{2}T(2\pi k\tau-\Omega_d)\left(1-\frac{|\tau|}{T}\right)\right)}{\frac{1}{2}T(2\pi k\tau-\Omega_d)\left(1-\frac{|\tau|}{T}\right)}\end{array}\right|^2 \tag{19}$$

where $|\tau| \le T$, τ is the time delay related to the distance and Ω_d is the frequency shift corresponding to the velocity. Fig. 4 shows the comparison of the single-chirp signal and the dual-chirp signal. Fig. 4(a) is the time-frequency analysis of the signal-chirp signal from 9.2 GHz to 10.2 GHz, which is generated by the AWG. The ambiguity function in Fig. 4(b) shows a knife edge. In Fig. 4(c), the time-frequency analysis of the dual-chirp signal generated by the DPMZM shows that in the duration time, the bandwidth of the up and down-chirp signal is 1 GHz. In Fig. 4(d), the sidelobe of the ambiguity function is suppressed, and the peak of the function is the original point. So, the range-Doppler resolution can be developed using the dual-chirp signal.

The EC can divide the dual-chirp signal into two parts. One is sent to the free space through the TA, and the other is applied to the DDMZM (Fujitsu LU-MZM-DPSK-X). The echo signal,

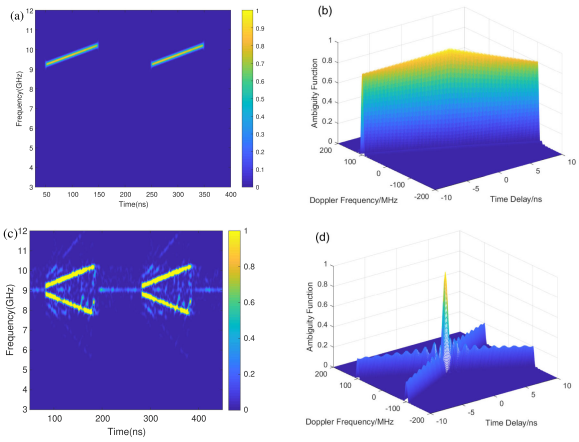

Fig. 4. The single-chirp LFM signal with a 1-GHz bandwidth from 9.2 GHz to 10.2 GHz (a) time-frequency analysis; (b) the ambiguity function. The dual-chirp LFM signal with two bands 7.8 GHz-8.8 GHz and 9.2 GHz-10.2 GHz (c) time-frequency analysis; (d) the ambiguity function.

which carries the distance information, is then collected by the RA and injected into the DDMZM after the EA (AV80212) to realize the de-chirping process. In the experiment, the gain of EA is 25 dB, and the bandwidth is 1 to 26.5 GHz. The bit rate and the amplitude of the PRBS are 2 Gb/s and 1 V, respectively. It is applied to the MZM3 for signal mixing.

In the experiment, the delay time caused by the experiment devices should be considered and measured. First, a reference distance is fixed and a series of distance measurements are based on it. The PD2 (Finisar XPDV2120RA) which has a 3-dB bandwidth of 40 GHz with a responsivity of 0.65 A W, transformed optical signal after the DDMZM into the electric signal and send it to the oscilloscope. The low-frequency interference can be filtered by electric filters. The sampling rate of the oscilloscope is set as 400 MSa/s, and the de-chirped frequency is measured to be 95.465 MHz. In the follow-up experiment, this value is described as the reference frequency. When the distance of the target is set as 51.0 cm, based on (8), the de-chirped frequency is 119.465 MHz. Fig. 5(a) shows the frequency domain of the de-chirped signal (black line), and the peak frequency value is 120.503 MHz. The distance of the target is measured as 52.557 cm. Based on the power spectrum of the de-chirped signal in Fig. 5(b) (black line). The signal power is calculated as -1.131 dBm and the noise power is calculated as -25.196 dBm, so the SNR is 24.065 dB. At this moment, the sampling point N $= 4096$.

To realize the compressive sampling process, the de-chirped signal and the PRBS which are both collected by the oscilloscope can be mixed and down-sampled by the computing platform. After the signal mixing, when the sampling rate of the oscilloscope is 200 MSa/s, in other words, the compressive sampling point M=2048 (M=N/2), the reconstruction process can be finished by using the CoSaMP algorithm, and the recovered de-chirped signal of the frequency domain is shown in Fig. 5(a) (red line). The peak frequency value of the recovered de-chirped signals is 120.503 MHz. According to the recovered peak frequency, the distances of the target can be calculated as 52.557 cm. The error

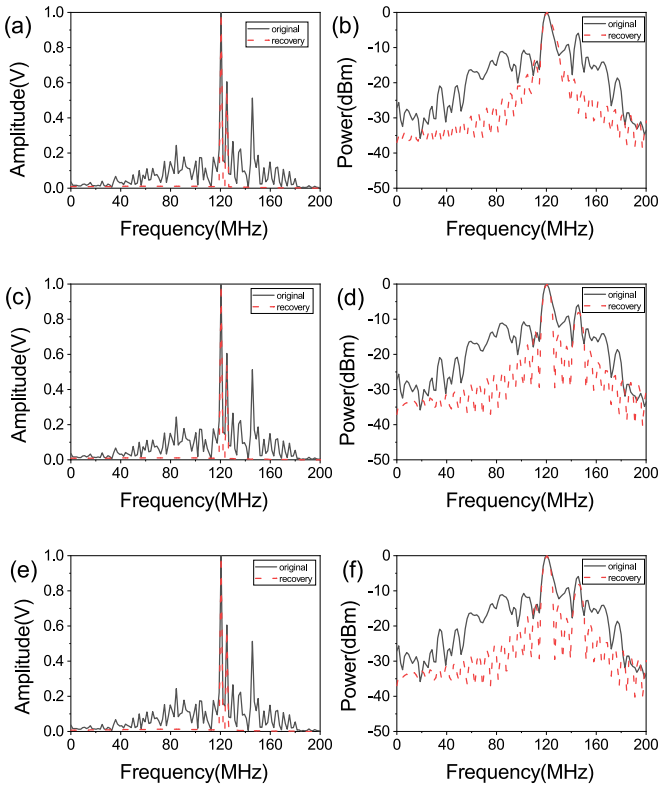

Fig. 5. Static target. Columns (a)–(e): the frequency spectra of the original signal (black line) and the recovery signal (red line) when the sampling rate of the oscilloscope is (a) 200 MSa/s, (c)100 MSa/s, and (e) 50 MSa/s. Columns (b)–(f): the power spectra of the original signal (black line) and the recovery signal (red line) when the compressive bandwidth of the oscilloscope is (b) 200 MSa/s, (d) 100 MSa/s, and (f) 50 MSa/s.

between the actual and measured distances is 1.557 cm. The power spectrum of the recovered signal, as shown in Fig. 5(b) (red line), demonstrates that the signal power is −1.371 dBm, and the noise power is calculated as −32.096 dBm, so the SNR is 30.725 dB. When the sampling rate of the oscilloscope is 100 MSa/s, that is, M=1024 (M=N/4), the de-chirped signal in the frequency domain is depicted in Fig. 5(c) (red line). Compared with the frequency spectrum of the original signal (Fig. 5(c), black line), the de-chirped frequency of the recovered de-chirped signal using the CoSaMP algorithm is 120.503 MHz. The distance of the target can be calculated as 52.557 cm, and the error of the distance is 1.557 cm. In Fig. 5(d), the power spectrum (red line) shows that the signal power is −1.810 dBm and the noise power is calculated to be −31.644 dBm. So, the SNR is 29.834 dB. When the bandwidth of the oscilloscope is 50 MSa/s (M=N/8), the peak frequency value in Fig. 5(e) is 120.505 MHz (red line). The distance of the target is measured as 52.560 cm, and the error of the distance detection is 1.560 cm. In Fig. 5(f), compared with the original signal (black line), the signal power is −1.809 dBm and the noise power is calculated to be −31.641 dBm. So, the SNR is 29.832 dB (red line).

Based on the comparison of recovery error and frequency value, it is clear that if the sparsity is appropriately set, the algorithm can recover the de-chirped signal faithfully and suppress the noise. Therefore, the SNR is improved. The reconstruction

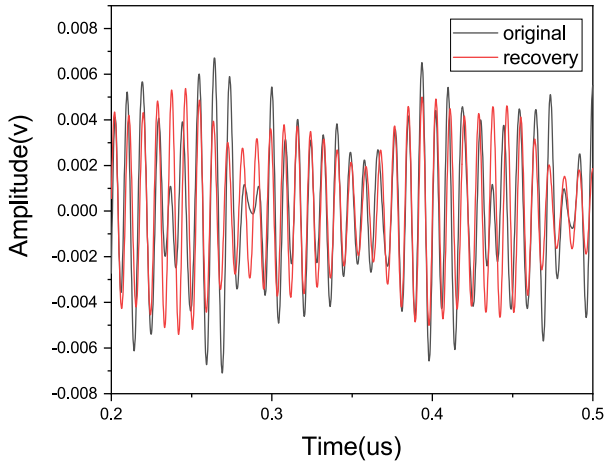

Fig. 6. The comparison of the time domain signal between the original signal (black line) and the recovery signal (red line).

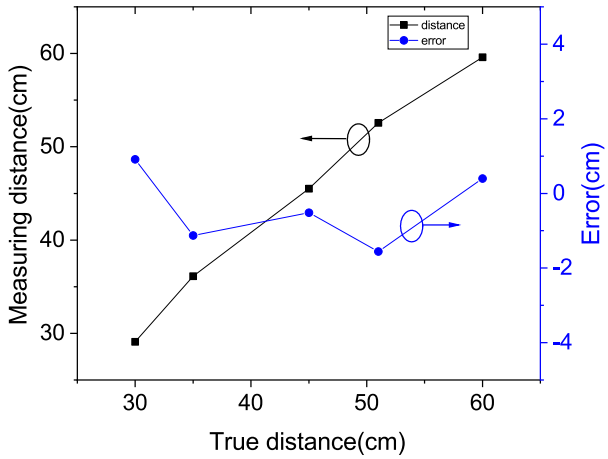

Fig. 7. The relationship and the error of the true distance and the measured distance.

result can be credible, and the distance of the target can be measured accurately under the sub-Nyquist sampling rate under a compressive factor of 8.

Fig. 6 shows the time domain signal comparison between the direct sampling and compressive sampling. It is seen that the time-domain performances of the original signal (black line) and the recovery signal (red line) show some differences. It is because the recovery of the noise signal is suppressed using CS technology, and the frequency of the de-chirped signal can not be influenced by the de-chirping process.

In the second experiment, the distance of the target changes from 30.0 cm, 35.0 cm, 45.0 cm, 51.0 cm, to 60.0 cm. The bandwidth of the oscilloscope is set as 50 MHz, corresponding to a compression ratio of 8. The measured distance is calculated according to the recovered frequency. The measured distance and the error related to the true distance are presented in Fig. 7. The measured distance is close to the true distance (black line). The maximum measured error is 1.560 cm (blue line).

When the target is moving, a series of simulations are performed. For the convenience of calculation, the distance and the velocity of the target are set as 15 m and 6 m/s, respectively.

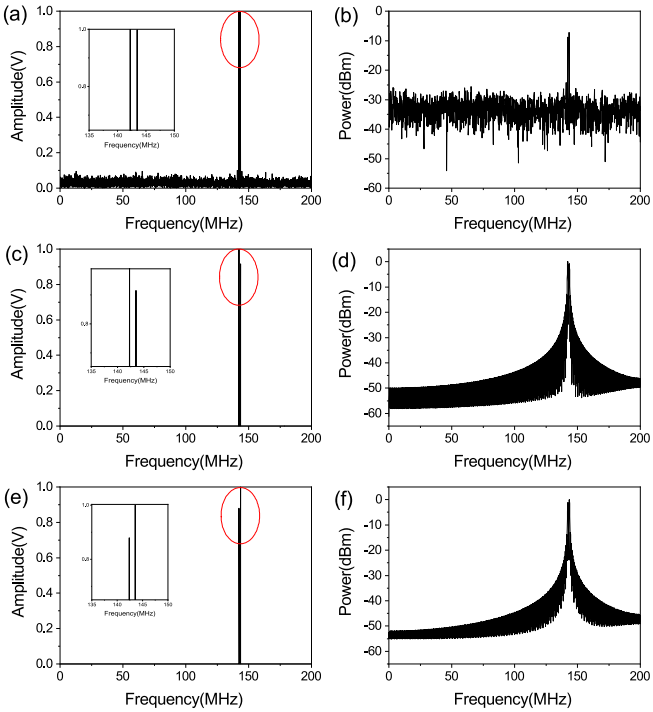

Fig. 8. Moving targets. (a) the frequency spectrum and (b) the power spectrum without CS technology. (c) the frequency spectrum and (d) the power spectrum with a compressive factor of 2. (e) the frequency spectrum and (f) the power spectrum with a compressive factor of 4.

The frequency range of the LFM signal generated from AWG is changed to 0–4 GHz, and the time duration of the LFM signal is 2.8 ms. The frequency of the RF signal is 15 GHz. After the DPMZM, the dual-chirped signal can be generated and the two bands are 11–15 GHz and 15–19 GHz. According to (9) and (10), the de-chirped frequency is influenced by the DFS. According to (11) and (12), the de-chirped frequencies are 142.257 kHz and 143.457 kHz, respectively. When the bandwidth of the ADC is 400 kHz (N=4096), as Fig. 8(a) shows, the de-chirped frequency values are 143.236 kHz and 143.357 kHz. Fig. 8(b) shows the power spectrum of the de-chirped signal. The signal power is −8.114 dBm and the noise power is calculated as −25.294 dBm. So, the SNR is calculated to be 17.180 dB.

Then the compressive factor is set as 2. Fig. 8(c) shows the frequency spectrum after the reconstruction process using the CoSaMP algorithm. In Fig. 8(c), the de-chirped frequencies are 142.285 kHz and 143.506 kHz, respectively. The distance is calculated to be 15.004 m, which indicates that the distance error is 0.4 cm. The velocity is calculated to be 6.105 m/s and the error is 0.105 m/s. In Fig. 8(d), the signal power is calculated to be −1.916 dBm and the noise power is calculated as −46.673 dBm. So, the SNR is 44.757 dB. Then, the compressive factor is set as 4. The de-chirped frequencies in Fig. 8(e) are 142.383 kHz and 143.555 kHz, respectively. As a result, the distance is calculated as 15.012 m, and the distance error is 1.2 cm. The target's velocity is 5.860 m/s and the error is 0.140 m/s. In Fig. 8(f), the signal power is −1.955 dBm and the noise power can be calculated as −46.580 dBm. The SNR is increased to 44.625 dB. For the comparison of frequency spectrums, compressive sampling and reconstruction can accurately recover the de-chirped signal with the DFS. In addition, the recovery of clutter can be suppressed. The power of the noise signal can be suppressed and the SNR is developed after the reconstruction.

A compressive sensing radar can be used in the car safety system. The compressive sensing radar can be combined with digital cameras and sensor systems to realize a full-angle target detection and environment sensing. The range resolution can be developed by adjusting the bandwidth of the transmitted signal. Moreover, an advanced vehicle driver assistance system can be set up. When the distance of the target is long, the power of the echo signal can be low to collect or submersed in the background noises. So, the SNR of the echo signal should be developed in a long-distance measurement. To develop the SNR of the echo signal, we can use a low noise amplifier after the receiving antenna. In addition, the filters can be used after the receiving antenna. The threshold value of the power detection can be appropriately set to filter the noise. If the SNR of the echo signal is developed and the compressive ratio is suitable, this system is fit for a long-distance measurement.

IV. Conclusion

In summary, we have proposed a dual-chirp microwave photonic radar based on CS technology to measure the distance and velocity of a target. The use of a dual-chirp signal is immune to the range-Doppler coupling. The central frequency and the bandwidth of the dual-chirp signal can be adjusted freely. In the receiving part, the system realizes the all-optical process for de-chirping and signal mixing, using the cascaded DDMZM and MZM. The results show that the de-chirped signal can be recovered accurately with a compressive factor of 8. In our experiment test, for a static target, the results of distance measurement can be measured accurately. The distance error is less than 1.560 cm. For a moving target, the simulation performance evaluates that the maximum distance error is 1.2 cm, and the velocity error is less than 0.140 m/s. If the sparsity is appropriately set, the noise signal can be suppressed, and the SNR can be developed to 30.725 dB. The CS microwave photonic radar shows excellent performance in distance and velocity measurement and great potential in 2-D image reconstruction, reducing the pressure of data storage and improving the speed of real-time imaging.

References

[1] R. Fitzgerald, "Effects of range-Doppler coupling on chirp radar tracking accuracy," *IEEE Trans. Aerosp. Electron. Syst.*, vol. AES-10, no. 4, pp. 528–532, Jul. 1974.

[2] L. Wang *et al.*, "Photonic generation and transmission of dual-band dual-chirp microwave waveforms at C-band and X-band with elimination of power fading," *IEEE Photon. J.*, vol. 13, no. 1, Feb. 2021, Art. no. 5500209.

[3] P. Ghelfi *et al.*, "Photonics for radars operating on multiple coherent bands," *J. Lightw. Technol.*, vol. 34, no. 2, pp. 500–507, Jan. 2016.

[4] S. Pan and Y. Zhang, "Microwave photonic radars," *J. Lightw. Technol.*, vol. 38, no. 19, pp. 5450–5484, Oct. 2020.

[5] F. Zhang *et al.*, "Photonics-based broadband radar for high-resolution and real-time inverse synthetic aperture imaging," *Opt. Exp.*, vol. 25, no. 14, pp. 16274–16281, 2017.

[6] H. Zhang *et al.*, "Photonic generation of linearly chirped microwave waveforms with tunable parameters," *IEEE Photon. Technol. Lett.*, vol. 32, no. 17, pp. 1037–1040, Sep. 2020.

[7] X. Li *et al.*, "Photonic generation of frequency and bandwidth multiplying dual-chirp microwave waveform," *IEEE Photon. J.*, vol. 9, no. 3, Jun. 2017, Art. no. 7104014.
[8] S. Zhu *et al.*, "Dual-chirp microwave waveform transmitter with elimination of power fading for one-to-multibase station fiber transmission," *Opt. Lett.*, vol. 45, no. 5, pp. 1285–1288, 2020.
[9] R. Cheng *et al.*, "Photonic generation of programmable coherent linear frequency modulated signal and its application in X-band radar system," *Opt. Exp.*, vol. 27, no. 26, pp. 37469–37480, 2019.
[10] Y. Xu *et al.*, "Photonic generation of dual-chirp waveforms with improved time-bandwidth product," *IEEE Photon. Technol. Lett.*, vol. 29, no. 15, pp. 1253–1256, Aug. 2017.
[11] J. Zhang *et al.*, "Photonics-based simultaneous measurement of distance and velocity using multi-band LFM microwave signals with opposite chirps," *Opt. Exp.*, vol. 27, no. 20, pp. 27580–27591, 2019.
[12] Y. Bae *et al.*, "X-band photonic-based pulsed radar architecture with a high range resolution," *Appl. Sci.-Basel*, vol. 10, no. 18, pp. 1–14, 2020.
[13] F. Yin *et al.*, "Multifrequency radio frequency sensing with photonics-assisted spectrum compression," *Opt. Lett.*, vol. 38, no. 21, pp. 4386–4388, 2013.
[14] Q. Guo *et al.*, "Compressive spectrum sensing of radar pulses based on photonic techniques," *Opt. Exp.*, vol. 23, no. 4, pp. 4517–4522, 2015.
[15] B. Yang *et al.*, "Broadband microwave spectrum sensing based on photonic RF channelization and compressive sampling," *IEEE Photon. J.*, vol. 12, no. 1, Feb. 2020, Art. no. 5500109.
[16] S. K. Sahoo and A. Makur, "Signal recovery from random measurements via extended orthogonal matching pursuit," *IEEE Trans. Signal Process.*, vol. 63, no. 10, pp. 2572–2581, May 2015.
[17] A. Chatterjee and P. W. T. Yuen, "Rapid estimation of orthogonal matching pursuit representation," in *Proc. IEEE Int. Geosci. Remote Sens. Symp.*, 2020, pp. 1315–1318.
[18] M. A. Davenport and M. B. Wakin, "Analysis of orthogonal matching pursuit using the restricted isometry property," *IEEE Trans. Inf. Theory*, vol. 56, no. 9, pp. 4395–4401, Sep. 2010.
[19] D. Needell and J. A. Tropp, "CoSaMP: Iterative signal recovery from incomplete and inaccurate samples," *Appl. Comput. Harmon. Anal.*, vol. 26, no. 3, pp. 301–321, 2009.
[20] D. Wu *et al.*, "The theory of compressive sensing matching pursuit considering time-domain noise with application to speech enhancement," *IEEE-ACM Trans. Audio Speech Lang.*, vol. 22, no. 3, pp. 682–696, Mar. 2014.
[21] Y. Ding *et al.*, "Microwave photonic radar for distance and velocity measurement based on optical mixing and compressive sensing," *Appl. Opt.*, vol. 60, no. 27, pp. 8534–8539, 2021.
[22] D. Zhu and J. Yao, "Dual-chirp microwave waveform generation using a dual-parallel Mach–Zehnder modulator," *IEEE Photon. Technol. Lett.*, vol. 27, no. 13, pp. 1410–1413, Jul. 2015.